Open Archive Toulouse Archive Ouverte (OATAO)

OATAO is an open access repository that collects the work of Toulouse researchers
and makes it freely available over the web where possible.

A fatigue multi-site cracks model using coalescence, short and long crack growth laws, for anodized aluminum alloys

M. Chaussumier[a],*, M. Shahzad[b], C. Mabru[b], R. Chieragatti[b], F. Rezaï-Aria[c]

[a] *Université de Toulouse; INSA, UPS, Mines Albi, ISAE; ICA (Institut Clément Ader), INSA, 135 Av. de Rangeuil, 31077 Toulouse Cedex 4, France*
[b] *Université de Toulouse; INSA, UPS, Mines Albi, ISAE; ICA (Institut Clément Ader), DMSM, 10 Av. Edouard Belin, BP54032, 31055 Toulouse Cedex 4, France*
[c] *Université de Toulouse; INSA, UPS, Mines Albi, ISAE; ICA (Institut Clément Ader), Campus Jarlard, F-81013 Albi, France*

Abstract

It has been shown that decrease of the fatigue life of aluminium alloys treated with anodization can be explained by the degradation of surface condition due to pickling. In order to predict fatigue life of anodized aluminium alloys, a multi-site crack growth model is developed by considering the pickling pits sites as initial flaws from which fatigue cracks develop. A map of the pickled surface is built from topography measurement with a contact profilometer. Then the pits are detected and their sizes are defined (depth, length and width). At the beginning of the calculation, a short crack growth law is used for crack having depths less than grain size. Then Paris long crack growth law is used. The coalescence of cracks is considered when their lengths increased by its crack tip plastic zone are large enough to interact with other neighbouring short cracks. The fatigue life is calculated for K_{max} achieving 70 % K_{IC}.

Keywords: anodizing; pits; fatigue; aluminium alloy; short crack; long crack

1. Introduction

Aluminum alloys 2xxx and 7xxx are extensively used in aeronautical industry due to their superior strength to weight ratios. As the natural oxide layer thickness is not sufficient to protect structure when subjected to severe environmental conditions, aluminium alloys are often anodized by electrolytic process that produces controlled columnar growth of amorphous aluminium oxide on the surface [1]. Despite the benefits obtained for wear and corrosion resistance, it has been observed an important decrease of the fatigue resistance [2–5]. This decrease seems to depend on stress level. Generally this reduction in fatigue life is attributed to the brittle as well as porous nature of oxide layer and the tensile residual stress induced during anodizing process [6,7]. It can also be attributed to the surface degradation by pickling process before anodizing. The pickling pits have been identified to accelerate crack

---

* Corresponding author.
E-mail address: michel.chaussumier@insa-toulouse.fr.

initiation [8–10]. In addition, it has been shown that this effect depends upon initial machining roughness: the more it is, the less the effect on fatigue life is [11].

The aim of this study is to compare several multi-crack propagation models for pickled specimens to experimental test results. These pits were initially identified on pickled plate specimens with topography measurement which allowed to define the number, the size (depth, length) of the pits and their respective position. Four approaches for predicting fatigue life have been used. In all approaches, the relative position of the pits has been considered. These approaches distinguish one from another by the initial flaws size, the applied stress level at the deepest point of the pit calculated with finite elements models built from topography measurement, and the propagation law. In the last approach, we used the local stress concentration at the deepest point of the pit. This kind of approach has been already proposed for a two-dimensional model [12,13]. During their propagation, cracks emanating from pits can coalesce to form new crack front that then continue to propagate until cracks reach a critical size corresponding to $0.7 \, K_{IC}$.

2. Experimental Procedures

2.1. Materials

The material investigated in this work is 7010-T7451 aluminium alloy whose chemical composition is given in Tab. 1. It was provided in rolled plate form of 70 mm thickness. Microstructural investigations revealed the presence of unrecrystallized and recrystallized grains. The latter are highly elongated in the rolling direction as shown in Fig. 1. Grain size is about 350 µm in the rolling direction and about 150 µm and 60 µm in TC and TL directions respectively. Only two types of inclusions were mainly found in this material (Mg_2Si, Al_7Cu_2Fe) that were generally located in recrystallized grains. The average size of these particles varied between 8 to 10 µm. Mechanical properties of this alloy in the rolling direction are; yield strength 464MPa, ultimate tensile strength 526 MPa, Young's modulus 70.7 GPa and elongation 9.8%.

Table 1. chemical composition of 7010 Aluminium alloy

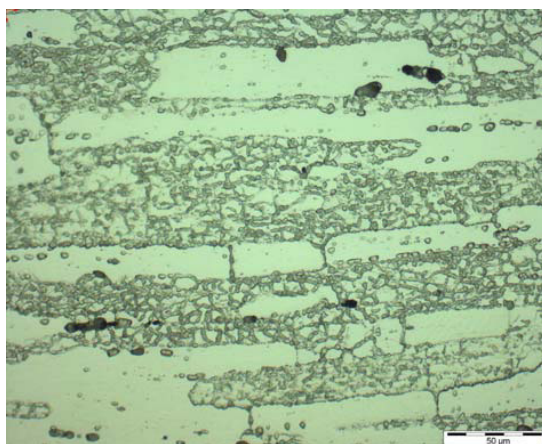| Element	Si	Fe	Cu	Mn	Mg	Cr	Zn	Zr	Ti
Weight%	0.12	0.22	1.98	0.20	2.86	0.15	6.45	0.27	0.14

Fig. 1. Microstructure of 7010-T7451.

2.2. Fatigue specimen preparation

Cylindrical test specimens were prepared in such a way that maximum load is applied perpendicular to the rolling direction, as shown in Fig. 2. They have been machined by turning without using lubricant. Turning was performed on 2 axes numerical lathe RAMO RTN20. Two types of machined surfaces (R_a=0.6µm and R_a=3.2µm) were produced. Machining conditions are shown in Tab. 2.

Fig. 2. Fatigue specimens position.
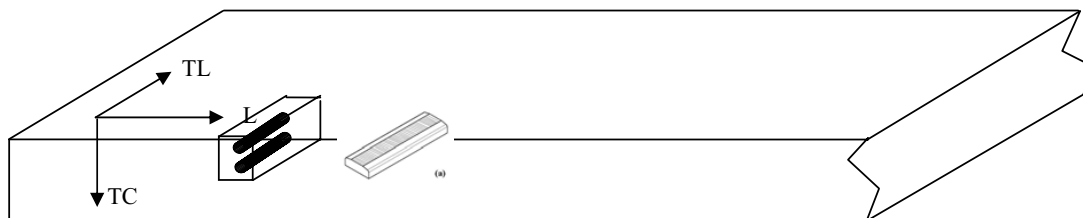
Table 2. Specimens machining conditions

Ra (µm)	Vc (m/min)	f (mm/tr)	p (mm)	ρ (mm)	lubrication
0,6	180	0,1	0,5	0,8	none
3,2	180	0,3	0,5	0,5	none

2.3. Surface treatments

For each initial roughness, specimens were categorized in 4 groups; the first group, with no treatment was used to build reference fatigue curve; the second group had specimens which undergone degreasing, the third group specimens were pickled and finally fourth one were anodized.

Specimens degreasing was carried out in aqueous solution of sodium tripolyphosphate $Na_2P_3O_4$ and Borax $Na_2B_4O_7$ at 60°C for 10–30 minutes followed by demineralised water rinsing. Pickling was done in aqueous solution of H_2SO_4 acid and anhydride chrome CrO_3 at 60°C between 1–10 minutes followed by rinsing. Chromic acid anodization was accomplished in anhydride chrome CrO_3 solution at 45°C under 50 volts for 55 minutes. The average thickness of oxide layer produced by the process was measured to be about 3µm

2.4. Surface measurement

Comparable surface roughness to that produced by turning of the cylindrical rotating bending specimens has been reproduced on plate specimens in order to better measure surface topography after pickling process. These surfaces have been obtained machined by a shaper with the same parameters as turning or for preparation of surface treated, especially in pickling process. Then surface topography measurements have been done using Mahr PKG120 profilometer. It is a conical diamond stylus instrument (90°– 2 µm radius) that can give conventional roughness parameters with horizontal and vertical resolutions of 0.5 µm and 0.1µm respectively. Several 2×2 mm^2 areas have been measured in order to lead a statistical analysis of the pickling pits. Specimens were placed on profilometer table such as the measurement directions correspond with applied stress direction. The resolution in this direction and in the transverse one is chosen equal to 5 µm. Pits characterisation is realised with a specific program. From the surface topography data, a plane orientation correction is made using the least square method. In this step, pits are neglected in face of the selected area and normal distribution factor is calculated. Then, surface profile, calculated from machining conditions, is subtracted from the real surface. The depth of the pits is defined from this new surface under the following condition:

$$z_{ij} - \hat{z}_{ij} < Ra \qquad (1)$$

where z_{ij} represents the measured depth, $\hat{z}_{ij}$ the theoretical depth considering machining conditions and Ra represents the arithmetic average roughness.

All adjacent points matching the above condition are assumed to belong to the same pit. By this way, each pit can be characterised through its maximal depth, its length (along transverse direction) and width (along applied stress direction) but also its position on the surface. Figure 3 illustrates this characterization method; pits are colored in red. Statistical treatments of this characterization allow establishing depth and length distribution graphs of pits.
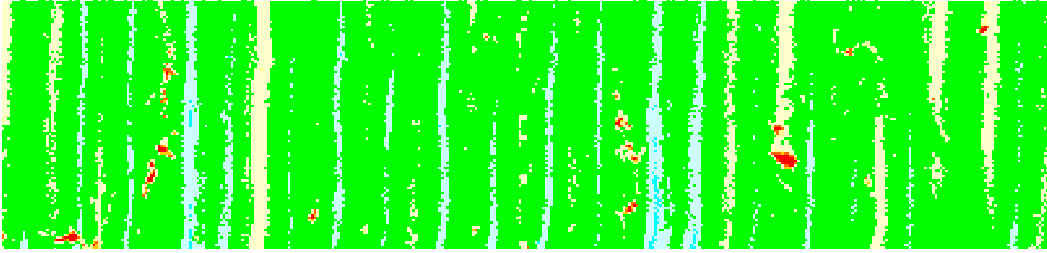

Fig. 3. Pickled surface topography for low roughness machining conditions.

3. Modeling

3.1. Finite elements models

From corrected surface topography, 3D finite elements models using the FE code Abaqus have been developed for each measured area. Linear bricks elements with 8 nodes have been used. The element size corresponds to the resolution used for topography measurement in each direction of the surface. The local surface crater depths correspond exactly to the measured depths. The thickness of the meshed volume, the number of elements trough the thickness and the ratio between element thickness are then defined. Displacements in the direction of applied stress are applied on the extreme transverse section of the finite element model. These models allow calculating for each pit a local mean stress, denoted $\sigma_{i,loc}^{max}$. Then, for each pit, a stress concentration factor Kt_i is defined as:

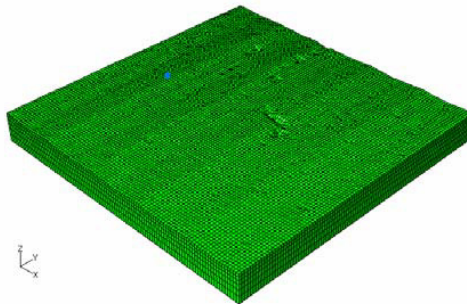$$Kt_i = \frac{\sigma_{i,loc}^{max}}{\sigma_{nom}^{max}} \qquad (2)$$

Fig. 4. Finite element model constructed from surface topography.

3.2. Crack propagation models

In order to predict the fatigue life, an analytic model has been developed based on linear fracture mechanics with local plasticity correction. In this model, each pickling pit is considered as a semi-elliptical micro crack with a shape factor c/a. Four approaches have been developed with considering the crack coalescence. The crack propagations on surface and inward the width of the specimen are calculated simultaneously. However the initial size of cracks and the fatigue crack growth law are different for each approach.

3.2.1. Modeling of crack coalescence

Crack propagation rate of a crack is influenced by the proximity of other cracks [14]. During propagation, cracks interact with each other even if the crack tips do not touch each other. At this state of the development of the model, two cracks become a single crack without being necessary a semi-elliptical crack. During the coalescence step, the single cracks transform to semi-elliptical cracks. Then a single crack propagates until it interacts with another crack and so on. We consider the coalescence is occurring when the crack tip plastic zones of two cracks touching each other. This coalescence condition depends on the relative position of the two cracks. For example, if one of the cracks is entirely on one side of the other one, the condition of coalescence can be expressed as follow:

$$d_{ij} \leq zp_i + zp_j$$

$$zp = \frac{1}{\pi} \cdot \left(\frac{K^{\max}}{Rp} \right)^2 \qquad (3)$$

$$d_{ij} = \sqrt{(x_{i_i} - x_j)^2 + (y_i + c_i - y_j - c_j)^2}$$
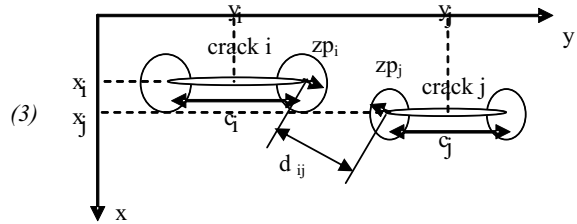

Fig. 5. Coalescence criteria conventions.

3.2.2. Propagation models

The first approach consists in considering only the multicracks and coalescence of long fatigue cracks emanating from the pits. The size of initial flaw is calculated using Kitagawa relation between stress intensity factor threshold ΔK_{th} and fatigue limit σ_D

$$a_0 = \frac{1}{\pi} \cdot \left(\frac{\Delta K_{th0}}{(1-R) \cdot \sigma_D} \right)^2 \qquad (4)$$

In this first approach, it is considered that the initial flaw depth is grater than the pit depths. In this condition the local stress at the deepest point of the crack front is considered to be equal to nominal stress. Therefore local stress raising is not taken into account and thus the local stress factor is 1. On the contrary, the stress concentration factor at the surface is considered by using Kt_{local} method [15]. The propagation is calculated using a long crack growth rate law. In order to predict more realistic the life, the crack initiation life (N_i) and propagation life (N_p) are considered. The S-Ni curves machined specimens [16] are obtained by:

$$N_i = N_R - N_p \qquad (5)$$

where N_p is calculated using the long crack growth law.

In the second approach, the size of the pits is considered but the stress concentration factor is still neglected. Alike the first approach, the stress concentration factor on surface with a particular roughness due to machining, is considered and again the propagation law is calculated as the approach 1.

In the third approach, the size of the pits is set as initial flaw size and the stress concentration factor at the deepest point of the pits is also considered. Two stages of propagation are considered. In the first stage, the stress concentration factor at the maximum depth of pit controls the crack growth rate. This stress concentration factor has been calculated using previously mentioned FEM model. In the second stage the cracks shape factor c/a, is taken into account for the crack growth. This consideration is intuitively in according with the experimental evidences of small cracks propagation. Several studies on aluminium alloys have shown that micro cracks could propagate even if the stress intensity factor range ΔK is less than the threshold stress intensity factor range ΔK_{th} usefully defined for long cracks [17,18]. It is often observed that short crack growth rate is greater than the long crack for given range of stress intensity factor less than ΔK_{th}. Furthermore, for some small cracks the propagation can stop, for others, the crack growth rate first decrease and the increase to join long crack growth rate law. In this model, the transition between the two region of crack propagation is fixed to be ΔK_{th}. For stress intensity range factor less than ΔK_{th}, the stress concentration factor at the deepest point of the pit is consider while over ΔK_{th} the stress is equal to nominal stress.

In the last approach, a specific small fatigue crack growth rate law is associated to the first stage of crack growth. The small crack growth rate is calculated using ΔK_{th} corresponding to a pit depth a using El Hadad's model [19] based on Kitagawa's theory.

$$\Delta K_{th,a} = \Delta K_{th} \cdot \sqrt{\frac{a}{\dfrac{a_0}{\alpha^2} + a}} \tag{6}$$

where a_0 is given by Eq. 4.

α is the geometric factor at the deepest pits depth that is also depending on shape factor c/a. Then short crack growth rate $C_{fc,a}$ is calculated by reporting stress intensity factor range threshold $\Delta K_{th,a}$ into the long cracks growth rate law:

$$C_a = C \cdot \Delta K_{th,a}^m \tag{7}$$

where C et m are long crack Paris' law parameters. For the present alloy investigated, these parameters are equal to $3.17 \, 10^{-11}$ and 3.41, respectively with ΔK_{th} equal to 3.5 MPa$\sqrt{m}$ for a_0 about 200 μm [13].

Several models have been proposed for the calculation of the geometric factor α. In the present model, Murakami's geometrical correction factor is chosen due to its simplicity [20]. Figure 6 illustrate the evolution of this factor for the deepest depth of the crack and for the tip point at the surface. For the depth, the curve has been extrapolated for shape factor value over 2 and was limited to 0.2 as it can be seen (see white triangular points). For the surface, the correction factor has been limited to 1 for shape factor over 4.5.
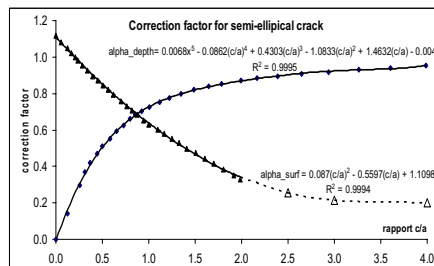

Fig. 6. Murakami's geometrical correction factor as function of shape factor c/a.

4. Results and discussion

Figure 7 illustrate fatigue life as a function of alternating stress for each group of test specimens. It can be observed an important decrease in fatigue life scattering between machined specimens and anodized specimens. This decrease depends on stress level. When the applied stress decreases this diminution becomes worth in accordance with literature. It can be also observed that fatigue life curves for pickled specimens and anodized specimens are much closer. That indicates the primacy of pickling on the global decrease of fatigue resistance of anodized specimens. All these results have been treated using Kt_{local} method. It has been shown that results for machined specimens, degreased ones and pickled ones are set on the same S-N curve, Fig. 8. The fracture surface of specimens with different treatments were examined by the SEM to identify the crack origin sites. The examination revealed multi-site crack initiation for the pickled and anodized specimens. The pickling pits initiating the fatigue cracks were about 8µm deep.

The statistical distribution of surface (2×2 mm^2) topography depth is shown in Fig. 9a. 117 pickling pits have been characterized at the surface of low initial roughness. Most of them are of small depth with an average being about 6 µm. Only 2% of these pits are more than 10 µm depths. In the same manner, the pit's mean length is about 10 µm (see Fig. 9b) and the longest ones are about 30 µm depth. Shape factor is between 0.58 and 3.28 with a mean value equal to 1.3. For 86% of the pits, the shape factor is less than 2.
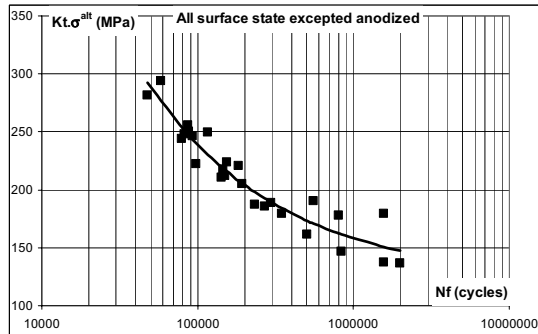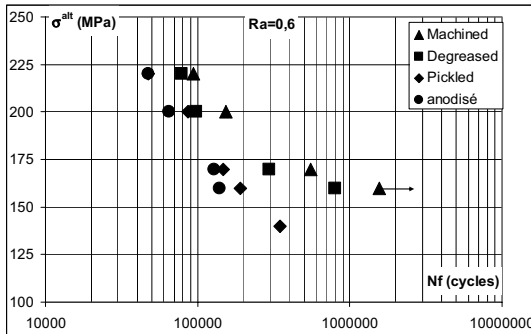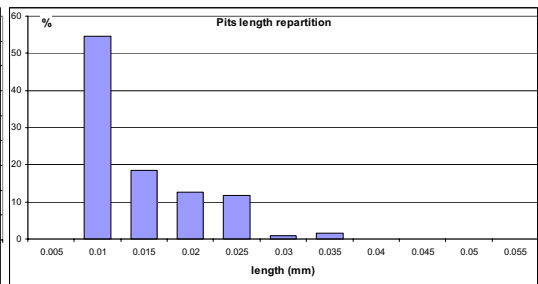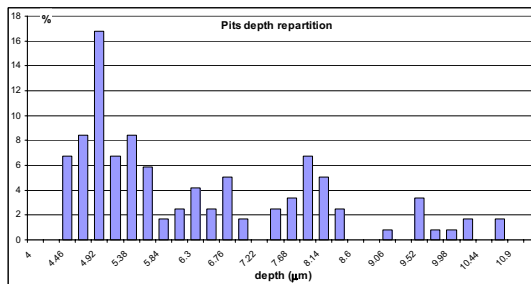

Fig. 7. Fatigue results for all the surface treatments and low roughness.

Fig. 8. Fatigue results using Kt_{local} method for all surface treatments excepted anodizing and for the two initial surface roughness.

(a)   (b)

Fig. 9. Pickling pits depth (a) and length (b)distribution graphs.

In the same way, it is possible to define the statistical distribution of stress concentration coefficient. Mean stress concentration coefficient is about 2.24. Figure 10 illustrates the results of one of these FEM models. Figure 11 presents stress concentration distribution for a given simulated area.
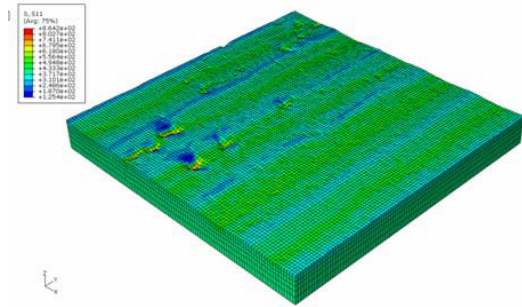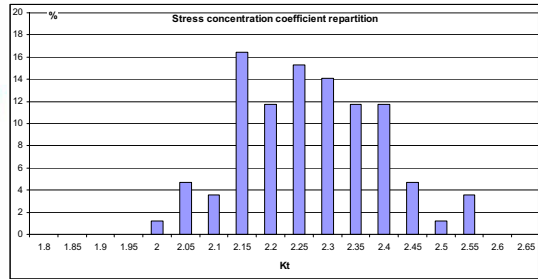
Fig. 10. Finite elements results.

Fig. 11. Statistical distribution of stress concentration coefficient.

The following figures illustrate the prediction of fatigue life given by the four approach presented in this paper. In the first approach, all the pits are considered and their respective position too. But their size is not considered. The size of the initial flaws is equal to the size of the crack corresponding to threshold stress intensity factor range. The effect of multicracks on propagation can be demonstrated through the decrease of Np of a single pit (Fig. 12). As it can be seen, the predicted fatigue life is lower than experimental life of the pickled specimens. However, initiation step is not considered in this approach. When correction factor is taken into account with the initiation curve, the predicted fatigue life is more close to the experimental data. The very good agreement obtained with this first model allows concluding on the importance of multicrack considerations associated with coalescence phenomena.

Figure 13 illustrates the results obtained with the second approach. As it can be seen, predicted life is very much optimist in comparison to the experimental results. This can be easily explained by the fact that the initiation step is not well represented because the actual stress at the pit's tip is not considered and also probably due to using an improper short crack growth rate law.

The predictions given with the third model are also too optimists comparing to experimental results but are more closed as it can be seen in Fig. 14. In this model, the influence of stress concentration at the pits until size reach a same critical size and the use of a single long propagation crack growth rate law reduce the difference between predictions and results comparing to the second models

In the last model, small crack growth rate laws depending on initial size of pits are considered. The influence of stress concentration until the size of the crack rich a transition size depending on initial size of the pits are considered too. The predictions given by this last model are in very good agreement with experimental results as it can be seen in Fig. 15. Agreement is better when stress level is high where propagation period in total life is predominant. But life predictions become conservative for low level stress level where the crack initiation is
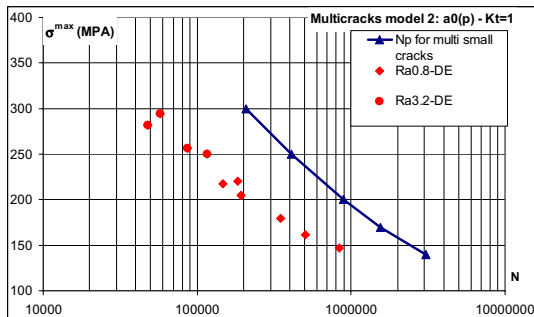

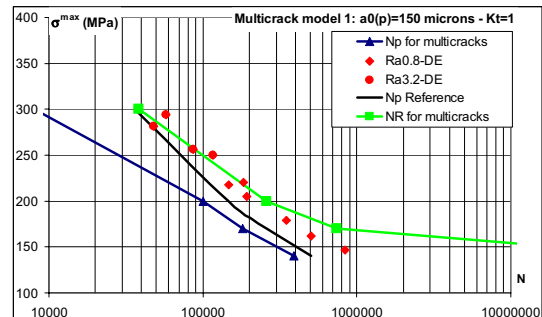Fig. 12. Fatigue life prediction given with model 1.

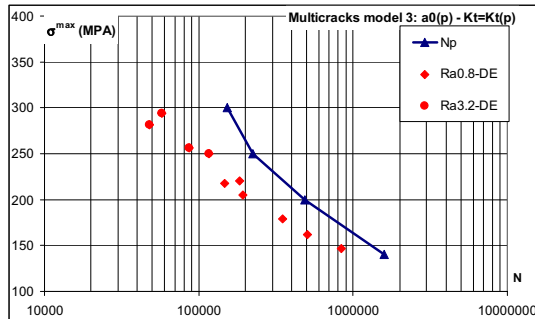Fig. 13. Fatigue life prediction given with model 2.

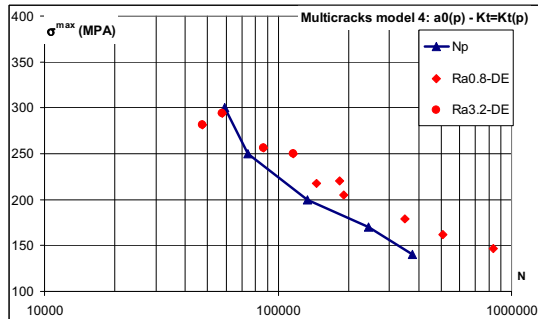Fig. 14. Fatigue life prediction given with model 3.

Fig. 15. Fatigue life prediction given with model 4.

predominant in total life. Such trend traduces the difficulty to characterize small crack growth rate. This is an important aspect to be investigated in the future.

5. Conclusion

Rotating bending fatigue test have been realized on aluminum alloy 7010 after machining, degreasing, pickling and anodizing. It has been observed an important decrease of fatigue life between machined specimens and anodized ones. It was also observed an importance effect of pickling on this decrease. Cracks initiate on pickling pits, (assimilated tt small cracks or flaws) and multicracks was observed. In order to predict the fatigue life of pickled specimens, a multicrack propagation model considering the coalescence of cracks has been developed. The depth and length repartition of pits have been characterized via surface topography measurements and statistical treatments. Finite elements models have been developed based on these same surface topographies in order to calculate stress concentration coefficient at the pits. It is considered that the local stress controls small cracks growth rate. Several approaches have been developed in order to distinguish the respective influence of the multicracking, the local stress effects and the small crack growth rate laws. The importance of multicracking coupled with coalescence of cracks is emphasized. The stress concentration at the bottom of pits and the small fatigue crack growth rate law seems equally play an important role. One of the further investigations will concern the small fatigue crack growth rate law characterizations.

6. References

[1] ASM Handbook, Corrosion, vol. 13, ASM International, USA, 1992.

[2] Cree AM, Weidmann GW. Effect of anodized coatings on fatigue cracks rates of aluminium alloy. *Surf Eng* 1997;**13**:51–5.

[3] Kermanidis AT, Petroyiannis PV, Pantelakis SG. Fatigue damage tolerance behaviour of coroded 2024 T351 aircraft aluminium alloy, *Theor Appl Fract Mech* 2005;**43**:121–32.

[4] Lonyuk B, Apachitei I, Duszczyk J. The effect of oxide coatings on fatigue properties of 7475-T6 aluminium alloy. *Surf Coat Tech* 2007;**201**:8688–94.

[5] Sadeler R. Effect of a commercial hard anodizing on the property of a 2024-T6 aluminium alloy. *J Mater Sci* 2006;**41**:5803–09.

[6] Camargo A, Voorwald H. Influence of anodization on the fatigue strength of 7050-T7451 aluminium alloy. *Fatigue Fract Engng Mater Sturct* 2007;**30**:993–1007.

[7] Cyrik E, Genel K. Effect of anodic oxidation on the fatigue performance of 7075-T6 alloy. *Surf Coat Tech* 2008;**202**:5190–201.

[8] Rokhlin SI, Kim JY, Nagy H, Zoofan B. Effect of pitting on fatigue crack initiation and fatigue life. *Eng Fract Mech* 1998;**62**:425–44.

[9] Pao PS, Gill SJ, Feng CR. On fatigue crack initiation from corrosion pits in 7075-T7351 aluminium alloy. *Scripta Mater* 1998;**43**:391–6.

[10] Dolley EJ, Wei RP. The effect of pitting corrosion on fatigue life. *Fatigue Fract Engng Mater Struct* 2000;**23**:555–60.

[11] Chaussumier M, Shahzad M, Mabru C, Chieragatti R, Rezaï-Aria F. Influence du décapage sur la tenue en fatigue de l'alliage Al7010-T7451 traité par oxidation anodique chromique, *19ème Congrès Français de Mécanique*, Marseille, 2009.

[12] As SK, Skallerud B, Tveiten BW, Holme B. Fatigue life prediction of machined components using finite element analysis of surface topography. *Int J Fatigue* 2005;**27**:1590–96.

[13] Suraratchaï M, Limido J, Mabru C, Chieragatti R. Modelling the influence of machined surface roughness on the fatigue life of aluminium alloy. *Int J Fatigue* 2008;**30**:2119–26.

[14] DeBartolo EA, Hillberry BM. Effects of constituent particle clusters on fatigue behaviour of 2024-T3 aluminium alloy. *Int J Fatigue* 1998;**20**:727–35.

[15] Chieragatti R, Surarachai M, Mabru C, Espinosa C, Vergnes V. *Procédés de caractérisation de la tenue en fatigue d'une pièce à partir de son profil de surface*. French Patent n°0650793, 2006.

[16] Santus C, Taylor D. Physically short crack propagation in metals during high cycle fatigue. *Int J Fatigue* 2009;**31**:1356–65.

[17] Pearson S. Initiation of fatigue cracks in commercial aluminium alloys and the subsequent propagation of very short cracks. *Eng Fract Mech* 1975;**7**:235–47.

[18] Lankford J. The influence of microstructure on the growth of small fatigue cracks. *Fatigue Fract Engng Mater Struct* 1985;**8**:161–75.

[19] El Haddad MH, Topper TH, Smith KN. Prediction of non propagating cracks. *Eng Fract Mech* 1979;**11**:573–84.

[20] Murakami Y, Nishitamni H. Stress intensity factor for interacting two equal semi-elliptical cracks in tension. *Trans Jap Soc Mech Eng Serv A* 1981;**47**:295–303.